



*SONO 2 SUB TYPES
dw DC cells*

AXL⁺SIGLEC6⁺ dendritic cells in cerebrospinal fluid and brain tissues of patients with autoimmune inflammatory demyelinating disease of CNS



Junho Kang ^{a,1}, Moonhang Kim ^{d,1}, Da-Young Yoon ^{c,1}, Woo-Seok Kim ^a, Seok-Jin Choi ^b, Young-Nam Kwon ^b, Won-Seok Kim ^b, Sung-Hye Park ^e, Jung-Joon Sung ^b, Myungsun Park ^a, Jung Seok Lee ^a, Jong-Eun Park ^{a,*}, Sung-Min Kim ^{b,*}, ²

^a Graduate School of Medical Science and Engineering, Korea Advanced Institute of Science and Technology, Daejeon, Republic of Korea

^b Department of Neurology, Seoul National University Hospital, Seoul National University of Medicine, Seoul, Republic of Korea

^c Department of Biomedical Sciences, Seoul National University College of Medicine, Seoul, Republic of Korea

^d Biomedical Research Institute, Seoul National University Hospital, Seoul, Republic of Korea

^e Department of Pathology, Seoul National University Hospital, Seoul National University of Medicine, Seoul, Republic of Korea

ARTICLE INFO

Keywords:

Inflammatory demyelinating disease
AXL⁺SIGLEC6⁺ dendritic cell
Single-cell RNA sequencing

ABSTRACT

Inflammatory demyelinating disease of the CNS (IDD) is a heterogeneous group of autoimmune diseases, and multiple sclerosis is the most common type. Dendritic cells (DCs), major antigen-presenting cells, have been proposed to play a central role in the pathogenesis of IDD. The AXL⁺SIGLEC6⁺ DC (ASDC) has been only recently identified in humans and has a high capability of T cell activation. Nevertheless, its contribution to CNS autoimmunity remains still obscure. Here, we aimed to identify the ASDC in diverse sample types from IDD patients and experimental autoimmune encephalomyelitis (EAE). A detailed analysis of DC subpopulations using single-cell transcriptomics for the paired cerebrospinal fluid (CSF) and blood samples of IDD patients (total $n = 9$) revealed that three subtypes of DCs (ASDCs, ACY3⁺ DCs, and LAMP3⁺ DCs) were overrepresented in CSF compared with their paired blood. Among these DCs, ASDCs were also more abundant in CSF of IDD patients than in controls, manifesting poly-adhesional and stimulatory characteristics. In the brain biopsied tissues of IDD patients, obtained at the acute attack of disease, ASDC were also frequently found in close contact with T cells. Lastly, the frequency of ASDC was found to be temporally more abundant in acute attack of disease both in CSF samples of IDD patients and in tissues of EAE, an animal model for CNS autoimmunity. Our analysis suggests that the ASDC might be involved in the pathogenesis of CNS autoimmunity.

1. Introduction

Inflammatory demyelinating diseases (IDDs) of the CNS are a group of autoimmune inflammatory diseases including not only multiple sclerosis (MS) [1], which accounts for the vast majority of IDD cases in western countries, but also antibody-mediated IDDs, comprising neuromyelitis optica spectrum disorder (NMOSD) and myelin oligodendrocyte glycoprotein antibody-associated disease (MOGAD) [2–4], which are more prevalent in Asian countries [5,6]. Due to the prevalence of T cells in active inflammatory plaque, MS has long been recognized as an autoimmune T cell-mediated disease [7]. Furthermore, the success of CD20-targeting antibody therapy has underscored the significance of B

cells in the pathology of the disease [8,9]. As a result, previous studies investigating MS pathophysiology and therapeutic targets have predominantly focused on T cells and B cells [8–12]. However, recent emerging evidence also suggests the importance of myeloid cells in IDD pathology [13–17].

DCs are professional antigen-presenting cells (APCs) that are drawing increasing attention as important players in autoimmunity [18,19], and mounting evidence indicates that DCs also play a critical role in the CNS in MS and experimental autoimmune encephalomyelitis (EAE) by activating pathogenic T cells [13,20,21]. Among APCs, CNS DCs play a greater role in activating myelin-specific T cells than microglia and macrophages in the mouse EAE model [22]. Considering that each DC

* Corresponding authors.

E-mail addresses: jp24@kaist.ac.kr (J.-E. Park), sueh916@gmail.com (S.-M. Kim).

¹ These authors contributed equally.

² These authors contributed equally.

subset exhibits distinctive functions, it is pivotal to comprehend the diversity of DC subsets to understand their specific role in disease. DCs were originally subclassified into plasmacytoid DCs and two conventional DC types (DC1 and DC2), according to their functional and morphological characteristics. Notably, recent advances in single-cell technologies have dramatically increased our sensitivity in classifying the heterogeneous DC populations, which led to the discovery of new DC subtypes such as AXL⁺SIGLEC6⁺ DCs (ASDCs) [23–25].

ASDCs were first discovered as a rare DC subpopulation in peripheral blood mononuclear cells (PBMCs) through DC-focused single-cell approaches. They are sometimes called transitional DCs (tDCs), due to their characteristic gene expression program which overlaps with DC2s and pDCs. In accordance with this phenotype, they can be activated by anti-CD40 and LPS stimulation and efficiently stimulate T cells [23–26]. In addition, their association with infection and inflammation has been shown in a mouse lung influenza infection model and in human skin inflammation [27,28]. However, the association of ASDCs with IDD pathogenesis has not been investigated in patients or experimental models.

To identify the diversity and the role of myeloid cells in IDDs at a high resolution, we have conducted a single-cell RNA sequencing (scRNA-seq) study of cerebrospinal fluid (CSF) and blood in two groups of IDDs (MS and antibody-mediated IDDs), with high sequencing depth and patient-wise coverage compared with a previously conducted MS study [11]. This allowed us to identify three DCs overrepresented in CSF (ASDCs, ACY3⁺ DCs, and LAMP3⁺ DCs) and discover the association between ASDCs and IDDs. Using the mouse EAE model, we also described the kinetics of the murine ASDC counterpart in disease pathology. Finally, we confirmed this finding in other autoimmune diseases, by identifying the association of ASDCs with tissue inflammation in patients with inflammatory bowel disease.

2. Materials and methods

2.1. Patient inclusion criteria and sample collection

For CSF samples, a total of 9 patients diagnosed with IDD, based on the diagnostic criteria (6 Ab-IDD and 3 MS), and 2 controls without inflammatory disease of the central nervous system (1 peripheral neuropathy and 1 degenerative neurological disease) were collected [29–31]. All CSF samples used for this study were provided from the Seoul National University Hospital. MS brain tissue was obtained from left parietal lobe from an MS patient at an attack stage (interval between onset and biopsy: 5 days), which was provided from the Brain Bank of the Seoul National University Hospital and Center for Medical Innovation (fig. S6B). Human normal brain was purchased from a commercial supplier (US Biomax, HuFPT020). Written informed consent were obtained from all participants in accordance with the Declaration of Helsinki (SNUH Institutional Review Board approval number: H-1902-083-1010, H-1908-038-1053).

CSF was quickly transported and centrifuged at 700g for 10 min. After centrifugation, the supernatant was removed, and then the pellet was resuspended with 30 µL of CSF. A total of 10 µL of the single-cell suspension was counted in a Cellometer counting chamber (PD100, Nexcelom, MA, USA) through staining with acridine orange and propidium iodide (AO/PI) reagent (CS2-0106, Nexcelom, MA, USA). Only samples having >2000 cells were selected for scRNA-seq. PBMCs were isolated using Lymphoprep (07861, STEMCELL Technologies, BC, Canada) and SepMate-50 tubes (ST86450, STEMCELL Technologies, BC, Canada) according to the manufacturer's protocol. Briefly, the enriched PBMCs were obtained from density gradient-medium centrifugation. The red blood cells were removed with an ACK lysing buffer (A1049201, Gibco, MA, USA). Cells were resuspended in complete RPMI medium containing 10% fetal bovine serum, 1% GlutaMax, and 1% penicillin/streptomycin up to 10 mL. All CSF/PBMC samples were processed without freezing in the RNA workflow.

2.2. Marker genes used for cell-type annotation

For T and innate leukocytes (ILC) including NK cells, we annotated naive CD4⁺ T cells (*CD4*, *SELL*, and *CCR7*), memory CD4⁺ T cells (*CD4*, *IL7R*, and *KLRB1*), Th1 (*CCL5* and *TBX21*), Th2 (*GATA3*), Th17 (*RORC* and *CISH*), T follicular helper cells (*Tfh*; *CXCR5* and *TIGIT*), naive CD8⁺ T cells (*CD8B* and *CCR7*), memory CD8⁺ T cells (*CD8B* and *CCL5*), resident memory T cells (*Trm*; *GZMK* and *NELL2*), effector memory T cells (*Tem*; *GZMB* and *KLRD1*), γδ T cells (*TRDC*), mucosal-associated invariant T cells (*MAIT*; *SLC4A10* and *CXCR6*), regulatory T cells (*Tregs*; *FOXP3* and *CTLA4*), CD16⁺ NK cells (*GNLY*, *FCGR3A*, and *PRF1*), XCL1⁺ NK cells (*GNLY* and *XCL1*), and ILCs (*TNFRSF4* and *IL1R1*).

B-cell clusters were divided into naive B cells (*MS4A1* and *IGHD*), memory B cells (*CD27*), and plasma B cells (*IGHG1* and *JCHAIN*). Myeloid cells expressing *LYZ* were separated into classical dendritic cells type 1 (DC1; *CLEC9A* and *XCR1*), classical dendritic cells type 2 (DC2; *CD1C*, *CLEC10A*, and *FCER1A*), AXL⁺SIGLEC6⁺ DCs (ASDC; *AXL*, *SIGLEC6*, and *PPP1R14A*), ACY3⁺ DCs (*ACY3*, *S100B*, and *CD1A*), LAMP3⁺ DCs (*LAMP3* and *CCR7*), microglia (*TMEM119*, *TREM2*, and *P2RY12*), CD14⁺ monocytes (*CD14* and *FCN1*), CD16⁺ monocytes (*FCGR3A* and *LST1*), neutrophils (*CXCR2*, *IFIT1*, and *FCGR3B*), and mast cells (*KIT* and *CPA3*). Additionally, plasmacytoid DCs (pDC; *IL3RA*, *CLEC4C*, and *JCHAIN*), megakaryocytes (Mgk; *GNG11* and *CLU*), and a small number of erythrocytes (*HBB*) were found.

2.3. Single-cell RNA sequencing experiment

Single-cell cDNA synthesis, amplification, and sequencing libraries were generated using the Single Cell 3' Reagent Kit (10× Genomics) following the manufacturer's instructions. Sequencing was carried out on an Illumina HiSeqXten and sequenced using the following parameters: Read1: 28 cycles, i7: 8 cycles, i5: 0 cycles, Read2: 91 cycles to generate paired-end reads.

2.4. Single-cell RNA sequencing data analysis

Droplet-based sequencing data were aligned and quantified using the Cell Ranger Single-Cell Software Suite (version 4.0.0, 10x Genomics Inc.) using the GRCh38 human reference genome (official Cell Ranger reference, version 2020-A). Cells with fewer than 2000 UMI counts and 500 detected genes were considered to be empty droplets and removed from the dataset. Cells with >7000 detected genes were considered as potential doublets and removed from the dataset. The Scanpy (version 1.8.1) Python package was used to load the cell-gene count matrix and for analysis [32]. Clustering, annotation, and downstream analysis were performed using the tools in the Scanpy package complemented with some custom codes. Scrublet was used for doublet detection [33], the batch correction was performed using the Harmony algorithm [34], and cell-cell interaction was assessed using CellPhoneDB and NicheNet [35,36].

2.5. Differential expression analysis (per-patient analysis)

We performed differentially expressed gene (DEG) analysis by calculating the mean gene expression of each individual (or samples) for every gene, considering each individual as one point to compare. Individuals with fewer than 10 cells were excluded for DEG analysis, and a t-test was used to calculate the p-values.

2.6. Cell type proportion analysis

Cell-type proportion calculations were performed after merging our dataset with the previous MS dataset, comprising a total of 15 IDD patients (Ab-IDD; n = 6, MS; n = 9) and 8 non-inflammatory controls (Figs. 1, D to G, 3C, and 4E, and figs. S2, B to E, and S5B). For cell-type proportion comparisons between different disease statuses and cell-type

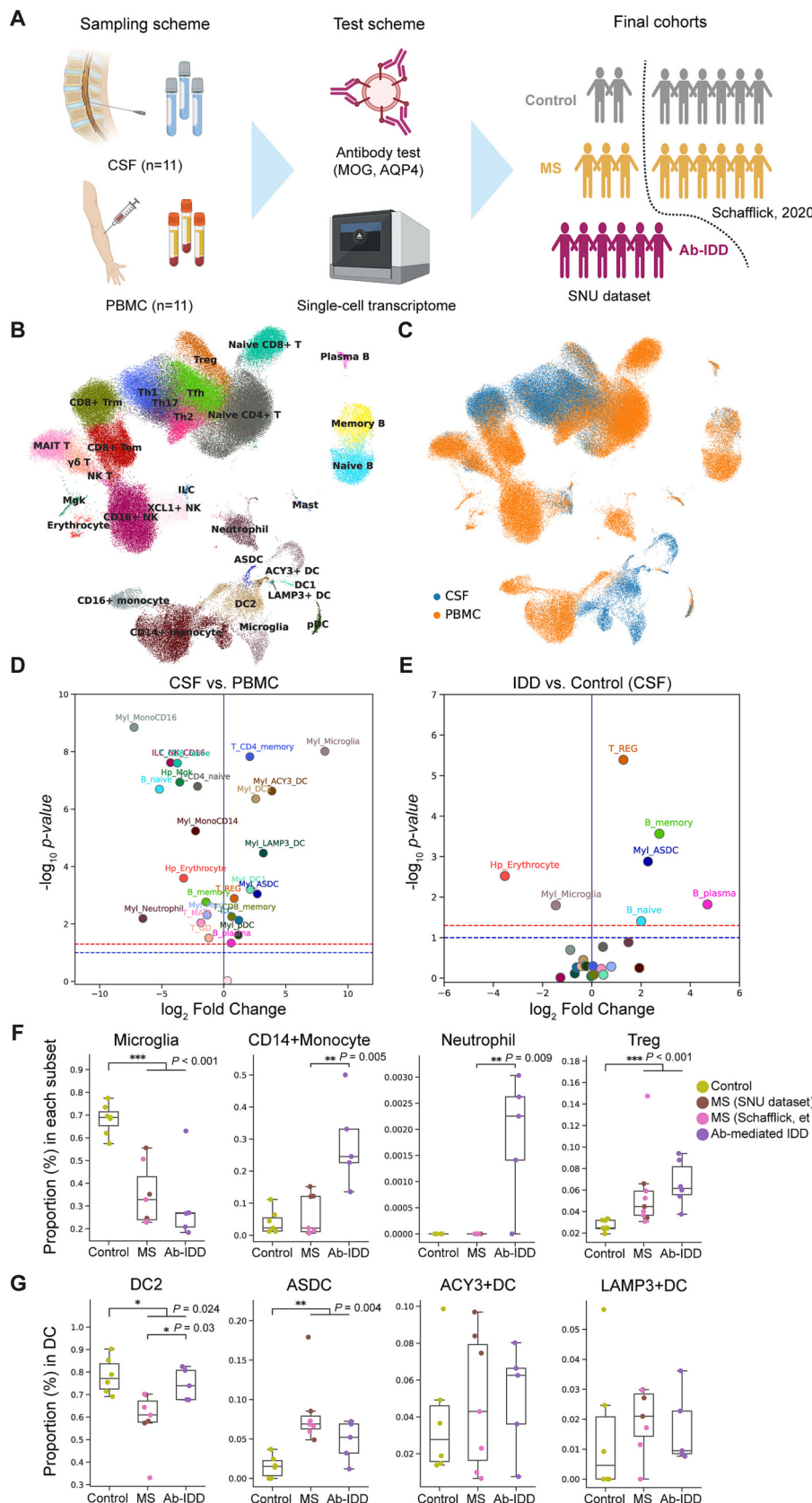


Fig. 1. Single-cell analysis of CSF with matched PBMC in inflammatory demyelinating diseases reveals novel myeloid populations in CSF.

(A) Scheme of single-cell transcriptome profiling of CSF with matched PBMCs in IDD patients and non-inflammatory controls.

(B and C) UMAP visualization of the composition of CSF ($n = 41,455$) and PBMC ($n = 92,901$) cells from the SNU dataset (MS $n = 3$, Antibody-mediated IDD $n = 6$, and non-inflammatory control $n = 2$) colored by cell type (B) and the site of sample collection (C). (D) Volcano plot showing the differences of cell type abundance between CSF and PBMCs, p -values calculated with the Mann–Whitney U test.

(E) Volcano plot showing the differences of cell type abundance in the CSF compartment between IDD and non-inflammatory controls, p -values calculated with the Mann–Whitney U test.

(F and G) Boxplot showing cell type proportions between different disease statuses. Cell type proportions were calculated as described in the Methods section, and p -values were calculated with the Mann–Whitney U test. * $p < 0.05$, ** $p < 0.01$, *** $p < 0.001$.

correlation analysis (Figs. 1, F and G, 3C, and 4E, and figs. S2, D and E, and S5B), the denominator used for cell-type proportion calculation was the superset of each cell type (e.g., Treg: all T cells plus innate leukocytes; microglia: all myeloid cells; ASDCs: all dendritic cells). Patients with fewer than 100, 100, and 50 cells for each superset of T cells plus innate leukocytes, myeloid cells, and dendritic cells, respectively, were removed before the proportion calculation.

2.7. Flow cytometric analysis

Paired CSF and PBMC from 8 patients diagnosed with MS and 6 non-inflammatory controls were collected (Table S2). Freshly thawed and washed PBMCs and CSF cells were blocked for 10 min at 4 °C with FcR Blocking Reagent (130–059–901, Miltenyi Biotec). Then, the cells were incubated for 20 min at 4 °C in the dark with staining cocktail, containing the fluorescently labeled antibodies diluted in the Brilliant Stain Buffer (563,794, BD Biosciences). The antibodies used for surface staining were as follows: anti-human CD117 (c-kit) (313,216, Biolegend), anti-human CD11c (563,026, BD Biosciences), anti-human CD123 (563,405, BD Biosciences), anti-human HLA-DR (563,696, BD Biosciences), anti-human CD14 (563,698, BD Biosciences), anti-human CD324 (E-Cadherin) (324,104, Biolegend), anti-human CD137L (4-1BB Ligand) (311,504, Biolegend), LIVE/DEAD™ Fixable Red Dead Cell Stain Kit, for 488 nm excitation (L34972, Thermo), anti-human CD3 (61–0038–42, Thermo), anti-human CD19 (61–0199–42, Thermo), anti-human TL1A (46–7911–82, Thermo), anti-human CD16 (557,744, BD Biosciences), anti-human Axl, anti-human Siglec-6/CD327 (17–1087–42, Thermo), and anti-human CD5 (563,516, BD Biosciences). Flow cytometry was performed on a BD LSR-II (BD Biosciences) and was analyzed using FlowJo v10.8.1 (FlowJo LLC, Ashland, OR). Patients with a minimum of 30 CD14-CD16- cells were included for final analysis.

2.8. RNA smFISH

RNA smFISH was performed on formalin-fixed paraffin-embedded sections of biopsied brain tissue of MS patient (Table S3) with probes for human *CD3*, *AXL*, *SIGLEC6*, following manufacturer's instructions (Advanced Cell Diagnostics, RNAscope® Multiplex Fluorescent Detection Reagents v2, 323,110). Briefly, sections were deparaffinized and pretreated with hydrogen peroxide, target retrieval and protease IV (Pretreatment Reagents, 322,381 and 322,000). C2, C3, C4 probes were diluted 1:50 in the C1 probe, hybridized for 2 h at 40 °C and washed twice in the wash buffer (RNAscope® Wash Buffer Reagents, 310,091). After probe hybridization, to form the signal amplification, a cascade of hybridization was performed by incubating with Multiplex FL v2 Amp1 (30 min), v2 Amp2 (30 min) and v2Amp3 (15 min) at 40 °C. Sections were incubated with v2-HRP-C1 for 15 min at 40 °C and washed twice in wash buffer for 2 min. OpalTM fluorophores (Opal 570, 620 and 690) were diluted 1:1500 in TSA buffer (RNAscope® Multiplex TSA Buffer, 322,809) and incubated for 30 min at 40 °C followed by 2 washes of 2 min and HRP blocker incubation for 30 min at 40 °C. Subsequently, v2-HRP-C3 and v2-HRP-C4 (ACD, 4-plex Ancillary kit, 323,120) were developed in the same way. v2-HRP-C4 (ACD, 4-plex Ancillary kit, 323,120) signal was additionally developed for the fourth probe. Finally, slides were counterstained and mounted (Invitrogen, Pro-LongTM Gold Antifade Mountant, P10144). Images were acquired using a STELLARIS8 confocal microscope (Leica) by ×20, ×40 and ×100 objective for scanning and high magnification. For quantifying cell types, we utilized built-in cell detection and single measurement classifier function from the QuPath software [37].

2.9. EAE mouse model induction and assessment

Female wild-type C57BL/6 J mice were purchased from Dae Han Bio Link Co., Ltd. Mice were housed under specific pathogen-free conditions

at the Department of Experimental Animal Research in Seoul National University Hospital (SNUH) Biomedical Research Institute. All breeding and experiments were approved by the SNUH Institutional Animal Care and Use Committee (IACUC).

Ten-week-old mice were immunized for EAE with a Hooke kit (Hooke laboratories, EK-2110, Lawrence, MA, USA) according to the manufacturer's instructions. Briefly, 0.1 mL of MOG35–55/CFA (complete Freund's adjuvant) emulsion was injected at the lower and upper back, subcutaneously. Each mouse was given two injections of PTX (200 ng per injection intraperitoneally) on days 0 and 1 of MOG immunization, respectively. Mouse weight and the clinical score were followed up from day 8 after the immunization. The EAE clinical score was assessed with a 0–5 point scoring system, as follows: 0 = no symptoms, 0.5 = weakness of tail tip, 1 = limp tail, 1.5 = slightly wobbly walking, 2 = wobbly walking, 2.5 = dragging of hind legs, 3 = paralysis of hind legs, 3.5 = complete paralysis of hind legs, 4 = partial front leg paralysis, 4.5 = complete forelimb paralysis, 5 = dead.

2.10. Single-cell dissociation and flow cytometry for the EAE mouse model tDC analysis

To isolate a single cell for flow cytometry, mice were sacrificed and transcardially perfused with cold PBS. Brain and spinal cord were isolated and digested with 0.5 mg/mL DNase (DN25, Sigma) and 0.3 mg/mL Liberase TL (05401020001, Roche) for 1 h at 37 °C and minced with the use of a 22G syringe needle. Homogenized tissue was passed through a 70-µm filter and centrifuged. Pellets were resuspended with 37% and 70% Percoll to form a gradient and centrifuged at 2800 rpm for 25 min without braking. Cells were obtained between the 37% and 70% Percoll layers and washed with PBS supplemented with 2% FBS. Spleen and inguinal LN (inLN) were dissociated mechanically and resuspended in cold PBS with 2% FBS. The single-cell suspension was passed through a 70-µm filter and centrifuged at 1800 rpm for 5 min. RBC lysis was applied for 5 min and the cells were washed with cold PBS supplemented with 2% FBS, if necessary.

Cells were stained for viability with DAPI for 30 min at 4 °C in the dark and washed. Afterward, cells were incubated with anti-CD16/32 antibody (101,302, Biolegend) to block the Fc receptor. The antibodies used for surface staining were as follows: anti-mouse CD11b (101,243, Biolegend), anti-mouse CD11c (117,317, Biolegend), anti-mouse CD19 (557,958, BD Biosciences) anti-mouse CD3 (100,215, Biolegend), anti-mouse B220/CD45R (103,241, Biolegend), anti-mouse Cx3cr1 (149,005, Biolegend), anti-mouse F4/80 (45–4801–82, Thermo), anti-mouse Ly6C (128,033, Biolegend), anti-mouse Ly6G (563,978, BD Biosciences), anti-mouse SiglecH (129,604, Biolegend), and anti-mouse Xcr1 (148,206, Biolegend). Cells were stained for 30 min at 4 °C in the dark and then washed. The sample was analyzed using a BD FACSymphony A3 and the data were acquired with FlowJo and DIVA software.

3. Results

3.1. Single-cell analysis of inflammatory demyelinating disease patients reveals novel myeloid populations in CSF

The previous single-cell landscape study on MS patients reported the existence of canonical pDC, DC1, and DC2 populations in patient blood and CSF [11]. Given the diversity of DC subpopulations revealed by recent single-cell studies and the rarity of newly identified DC subtypes [25,38], we hypothesized that the generation of a new single-cell dataset with improved coverage might increase the chance of identifying novel DC subtypes in IDD patients. To this end, we have generated a single-cell transcriptome dataset for paired CSF and PBMC samples from IDD patients, which include both those with MS and with antibody-mediated IDDs (Ab-IDD, including anti-MOG IgG⁺ MOGAD and anti-AQP4 IgG⁺ NMOSD, Fig. 1A). Compared with the existing MS dataset (referred as “previous MS dataset”), our dataset (SNU dataset) detected about a 2-

fold higher number of genes per cell and covers a larger number of cells (fig. S1, A and B). The increased cell coverage and sequencing depth have allowed us to classify cell types at a finer resolution (Fig. 1, B and C). For example, T-cell subtypes such as Th1, Th2, Th17, and Tfh cells were clearly separated in the SNU dataset and, in concordance with the previous MS study, Tfh cells were increased in the CSF of IDD patients (fig. S2, A to C) [11]. Notably, the SNU dataset features increased complexity in the myeloid cell populations, which allowed the identification of neutrophils and three additional DC subtypes (Fig. 1B).

To increase the statistical power of the analysis, we integrated the SNU dataset with the previous MS dataset by transferring our high-resolution cell labels [11]. While we could confidently transfer the annotation for myeloid cells, T-cell subset annotation of the previous MS dataset was hindered by limited resolution. To circumvent this problem, we have maintained two layers of annotations throughout the SNU dataset (high and low resolution), by combining T-cell memory subtypes. After combining the two datasets, we characterized cell types more abundant in CSF by comparing the cells of the CSF with PBMC. Memory CD4⁺ T cells, memory CD8⁺ cells, Tregs, DC1s, DC2s, and pDCs were increased in CSF as described in the previous MS study (Fig. 1D)

[11]. Moreover, microglial cells and three subtypes of DC that were not previously clearly defined in the CSF (ASDCs, ACY3⁺ DCs, and LAMP3⁺ DCs), were also highly overrepresented in the CSF. When comparing the cell proportions in the CSF compartment in IDDs with those in non-inflammatory controls, ASDCs, Tregs, and B cells were increased in IDD patients, in contrast to microglia, which constituted a smaller proportion in IDD patients (Fig. 1, E to G). Furthermore, there were no significant differences in cell proportions based on age or gender (fig. S2, D and E).

Next, we took a closer look at each cell type according to the disease subtypes by comparing its proportions in normal, MS, and Ab-IDD patients. We observed a high expression level of *IL-10*, an immunosuppressive cytokine, in microglia (fig. S4A) [39] and notably, microglia numbers were decreased in both MS and Ab-IDD patients ($p < 0.001$, Fig. 1F). In contrast, the numbers of Tregs and ASDCs were consistently increased in IDD patients ($p < 0.001$ and $p = 0.004$, respectively, Fig. 1, F and G). While upregulation of Tregs was observed in the previous MS study [11], the association of ASDCs with IDD patients has not been reported before, leading us to focus on this DC subtype in this study.

Lastly, we also characterized the differences between MS patients

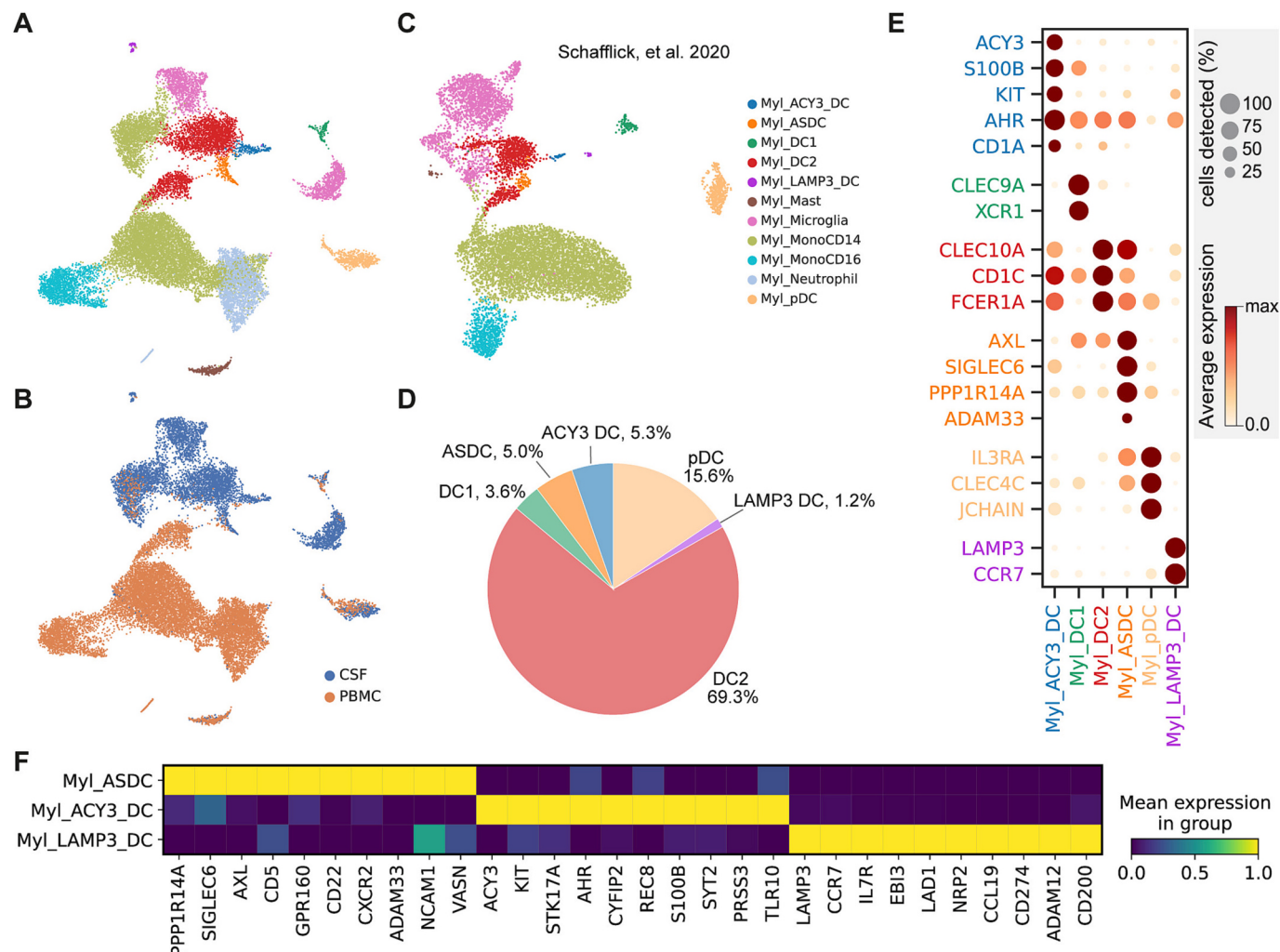


Fig. 2. Identification of myeloid cell subsets in inflammatory demyelinating disease characterizes tissue-resident dendritic cell subtypes overrepresented in CSF. (A and B) UMAP plot of secondary clustering of myeloid cells ($n = 19,233$) colored by cell types (A), and the site of sample collection (B). (C) UMAP plot of sub clustering of myeloid cells ($n = 10,394$) in the previous MS study also reveals tissue-resident DCs overrepresented in CSF. The cell types are colored the same as (A). (D) Pie chart showing the proportions of dendritic cell subtypes. (E) Dot plot for expression of marker genes in dendritic cell subtypes. Here and in later Fig., color represents the maximum-normalized mean expression of marker genes in each cell group, and size indicates the proportion of cells expressing marker genes. (F) Heatmap showing differentially expressed genes between each dendritic cell subtype overrepresented in CSF versus other DC subtypes.

and Ab-IDD patients, including the proportions of DC2s ($p = 0.03$), CD14⁺ monocytes ($p = 0.005$), and neutrophils ($p = 0.009$), highlighting the differences between MS and Ab-IDDs (Fig. 1, F and G).

3.2. Characterization of myeloid subtypes in the CSF of IDD patients

Having discovered DC subtypes that are overrepresented in CSF and associated with disease, we performed a secondary clustering of 19,233 myeloid cells (CSF $n = 6695$; PBMC $n = 12,538$) into 11 myeloid cell

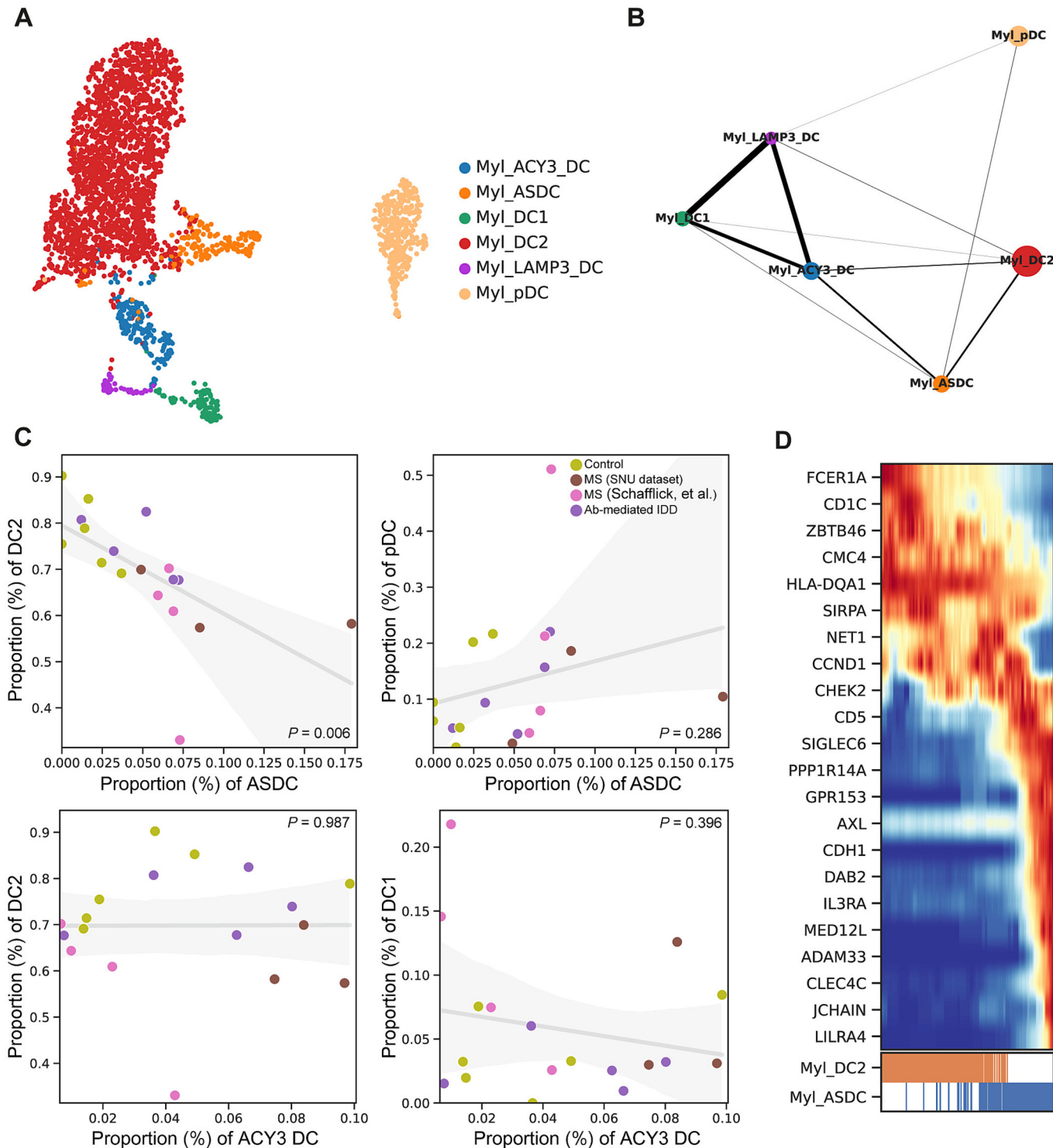


Fig. 3. The lineage relationship of tissue-resident dendritic cell subtypes overrepresented in CSF.

(A) UMAP plot of sub clustering of dendritic cells ($n = 2828$) in the CSF.

(B) PAGA graph showing connectivities between dendritic cells in the CSF.

(C) Scatterplot showing the relationship between the proportion of dendritic cell subtypes in each patient. Pearson correlation.

(D) Heat map showing differentially expressed genes across ASDC differentiation pseudotime. Top: The x-axis represents pseudo-temporal ordering. Gene expression levels across the pseudotime axis are maximum-normalized and smoothed. Bottom: Cell type annotation of cells aligned along the pseudotime axis.

clusters, including a novel ACY3-expressing DC type which had not previously been defined (Fig. 2A). Uniform Manifold Approximation and Projection (UMAP) presentation separated monocytes-enriched PBMCs from microglia- and DCs-enriched CSFs (Fig. 2B). The cell-type prediction on the public MS dataset based on our machine-learning classifier confirmed the existence of each cell type (Fig. 2C) [11]. In the CSF, DC2 was the most abundant DC subtype (69.3%), followed by pDCs (15.6%), ACY3⁺ DCs (5.3%), and ASDCs (5.0%, Fig. 2D).

To understand the characteristics of each DC subtype, we defined specific marker genes through differentially expressed gene (DEG) analysis (Fig. 2, E and F). Among newly identified DCs (ASDCs, ACY3⁺ DCs, and LAMP3⁺ DCs), ASDCs and ACY3⁺ DCs formed peninsula-like clusters sharing DC2-like signatures (*CD1C*, *FCER1A*, and *CLEC10A*). ASDCs also expressed pDC-like signatures (*IL3RA* and *CLEC4C*), along with *AXL*, *SIGLEC6*, and *PPP1R14A*, which were specific marker genes for ASDCs [25]. Marker genes for ACY3⁺ DCs included *ACY3*, *S100B*, *KIT*, and *AHR*. In comparison with DC2, ACY3⁺ DCs expressed *CD1A*, which can display a broad spectrum of exogenous lipid antigens derived from pollen or bacteria [40]. LAMP3⁺ DCs expressed high levels of *LAMP3* and *CCR7* (Fig. 2F), which are canonical marker genes for activated migratory DCs. Thus, our dataset allows the deep characterization of tissue-resident DCs overrepresented in CSF, revealing their unique gene expression programs.

3.3. Lineage relationship of tissue-resident DC subpopulations overrepresented in CSF

To investigate the lineage relationship between DC subtypes in CSF, we performed partition-based graph abstraction (PAGA) on CSF DC populations in the SNU dataset (Fig. 3, A and B) [41]. While ASDCs displayed transitional characteristics between DC2s and pDCs, UMAP projection and PAGA analysis consistently showed a closer association of ASDCs with DC2s (Fig. 3, A and B, and fig. S3, A and B). Interestingly, the proportion of ASDCs showed an inverse correlation with DC2s ($p = 0.006$), while not having any significant relationship with pDCs ($p = 0.286$, Fig. 3C), indicating the presence of lineage relationships between DC2s and ASDCs. To investigate the transcriptional relationship between ASDCs and DC2s in more detail, we performed pseudotime analysis using diffusion pseudotime, which resulted in an ordering of cells consistent with the known marker genes of DC2s, ASDCs, and pDCs (Fig. 3D and fig. S3C).

Similar to ASDCs, ACY3⁺ DCs expressed *SIGLEC6* and *TNFSF15* (Fig. 2E and fig. S4A) and shared many expression markers with DC2s (*CD1C* and *CLEC10A*). In addition, PAGA analysis connected them with DC1s and LAMP3⁺ DCs (Fig. 3B). ACY3⁺ DCs, DC1s, and LAMP3⁺ DCs all express high levels of *IDO1*, which encodes a metabolic enzyme with an immunosuppressive role (fig. S3D). In the population correlation analysis, ACY3⁺ DCs did not show any proportional correlation between DC2s ($p = 0.987$) or DC1s ($p = 0.396$, Fig. 3C). Notably, ACY3⁺ DCs can be further subdivided into two populations, which are marked by *CD1A* and *PIGR* expression, respectively (fig. S3D). Taken together, we observed a clear lineage relationship between ASDCs and DC2s, while ACY3⁺ DCs might have heterogeneous cell origin.

3.4. Cell interaction analysis shows poly-adhesional, stimulatory characteristic of ASDCs

To understand the functional characteristics of tissue-resident DCs overrepresented in CSF, we investigated the potential cellular interactions between each DC overrepresented in CSF with other cell types using cell-cell interaction inference tools such as CellPhoneDB and NicheNet, focusing on gene expression programs specific to these DCs (Fig. 4, A and B, and fig. S4, A to C) [35,36]. In this analysis, ASDCs expressed genes encoding various adhesion molecules known to be expressed in other cell types, including T cells (*CD5*), B cells (*CD22*), NK

cells (*NCAM1*), epithelial cells (*CDH1*), fibroblasts (*ADAM33*), smooth muscle cells (*ADAM33* and *VASN*), and erythroid cells (*ICAM4*, Fig. 4A). The glycoprotein *CD5* is usually expressed on the surface membrane of all mature T cells, known to specifically interact with *CD72*, which is expressed in naive B cells, ACY3⁺ DCs, DC1s, DC2s, and ASDCs in our study (Fig. 4A and fig. S4A) [42]. Therefore, *CD5*- and *CD72*-expressing ASDCs have the potential to interact with *CD72*-expressing naive B cells, ACY3⁺ DCs, DC1s, DC2s, and *CD5*-expressing T cells, and with themselves in homotypic aggregation (Fig. 4C). ASDCs also specifically express *CDH1* (E-cadherin), encoding an adherens junction protein that through homotypic interactions contributes to the maintenance of the epithelial barrier function (Fig. 4, A and C). Besides its role in adhesion, E-cadherin is a known modulator of several signaling pathways and influences the immunogenicity and tolerogenicity of DCs [43]. E-cadherin-expressing DCs have been associated with the pathogenesis of intestinal inflammation in T cell-mediated colitis, assuming a proinflammatory role of ASDCs [44]. *ICAM4* is strongly expressed on ASDCs and LAMP3⁺ DCs, binding to LFA-1 (*ITGAL*) and VLA-4 (*ITGA4*) integrins widely expressed on various immune cells (Fig. 4A and fig. S4A). LFA-1 and VLA-4 not only participate in multiple immune cell interactions, but also mediate the transendothelial migration in the CNS and immune cell recruitment to the site of inflammation [45,46]. This implies that ASDCs and LAMP3⁺ DCs may play a pivotal role in the recruitment of immune cells, leading to the onset of inflammation in the CNS.

In addition, ASDCs also express TNF superfamily genes which can stimulate other immune cells. ASDCs strongly express *TNFSF9*, which interacts with *TNFRSF9* expressed on LAMP3⁺ DCs. *TNFSF9* (4-1BB-L) has been shown to directly activate DC and enhance *IL-12B* expression in APCs, which suggests the stimulatory potential of ASDCs on LAMP3⁺ DCs that lead to IL-12 production (Fig. 4, B and D, and fig. S4A) [47,48]. In addition, ASDCs and ACY3⁺ DCs express *TNFSF15* (TL1A), which binds to *TNFRSF25* and induces costimulation of memory *CD4⁺* T cells (Fig. 4, B and D, and fig. S4, A to C) [49]. Interestingly, *TNFSF15* expression in ASDCs is primarily observed in CSF, which implies the acquisition of activated status for ASDCs in IDD patients (fig. S5A). Furthermore, in contrast to other cell types, the proportion of ASDCs were higher in patients in the attack stage (time from latest attack to sampling between 7 and 60 days), compared with the remission stage (time from latest attack to sampling after 60 days), implying its role as an acute phase reactant (Fig. 4E and fig. S5B). In summary, ASDCs are a poly-adhesional, disease-associated DC increased in the CSF at attack stage, and capable of stimulating *CD4⁺* T cells (*TNFSF15:TNFRSF25*) and LAMP3⁺ DCs (*TNFSF9:TNFRSF9*); binding to various immune cells (*ICAM4:ITGAL*, *ICAM4:ITGA4*) including B cells (*CD5:CD72*) and T cells (*CD72:CD5*); and also homotypic interactions (*CD5:CD72*, *CDH1:CDH1*), implying their potential role in the pathogenesis of the IDDS.

LAMP3⁺ DCs express various cytokines and chemokines, highlighting their activated status (Fig. 4B). LAMP3⁺ DCs interact with *CD4⁺* T cells and Tregs through *CCL17:CCR4*, *CCL22:CCR7*, and many co-stimulatory molecules (Fig. 4, B and D, and fig. S4A). Additionally, LAMP3⁺ DCs act as a B-cell chemoattractant by expressing *CXCL13* and binding to *CXCR5* on naive and memory B cells, enabling attraction to and recruitment of B cells into the CSF. LAMP3⁺ DCs also interact with plasma B cells orchestrated by the *CD70:CD27* axis, which is known to activate B cells and play a role in the course of inflammatory disease (e.g., EAE, arthritis, and inflammatory bowel disease; Fig. 4, B and D, and fig. S4A) [50,51]. In summary, with the interaction mediated through the *TNFSF9:TNFRSF9* axis, ASDCs and LAMP3⁺ DCs form an adhesive and stimulatory network priming autoreactive *CD4⁺* T cells and B cells in the CNS during the course of IDD pathogenesis.

3.5. ASDCs expand in the CSF of IDD patients and are associated with IDD pathology

We next tested whether ASDCs are altered in the CSF in IDD patients

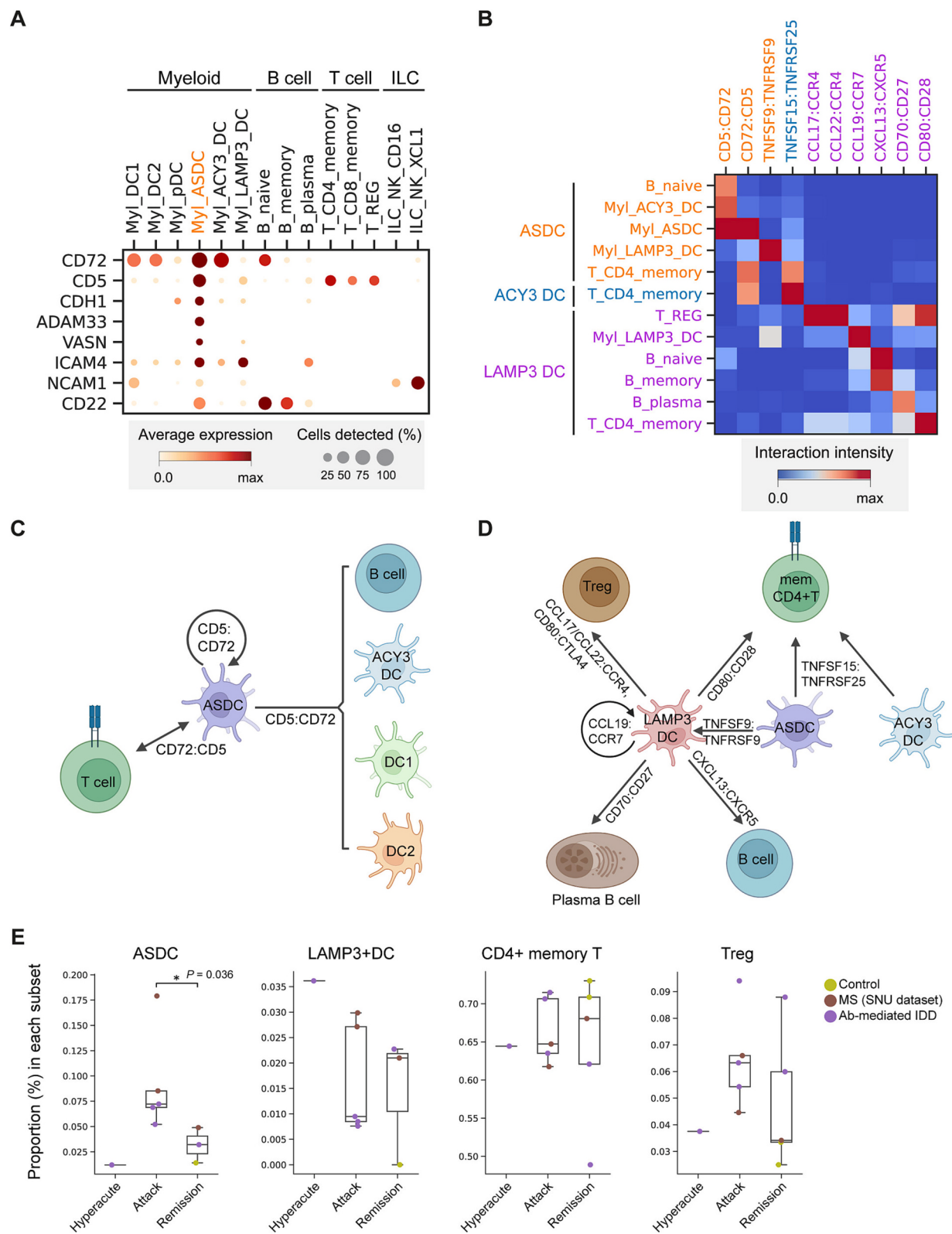


Fig. 4. Cell interaction analysis of dendritic cell subtypes overrepresented in CSF.

(A) Dot plot showing marker gene expressions of adhesion molecules expressed in ASDCs, in the CSF of IDD patients.

(B) Heat map of immune cell interactions in the CSF of IDD patients. Interaction intensity was calculated by multiplying the normalized expression value of ligand and receptors in each cell-cell pair.

(C) Schematic model summarizing the adhesion molecule interactions of ASDCs and other cell types.

(D) Schematic model summarizing the interactions of DCs overrepresented in CSF and other cell types.

(E) Boxplot showing cell type proportions according to time from latest attack to sampling. Cell type proportions were calculated as described in the Methods section, and p-values were calculated with the Mann-Whitney U test. *p < 0.05, **p < 0.01, ***p < 0.001.

and its association with IDD pathology. We identified AXL⁺SIGLEC6⁺ ASDC cells in the CSF by flow cytometry and found a significant enrichment of ASDCs in the CSF of IDD patients ($p = 0.002$), in accordance with our scRNA-seq analysis (Fig. 5, A and B). CDH1 ($p = 0.002$), TNFSF9 ($p < 0.001$), and TNFSF15 ($p = 0.04$) were also increased in the CSF (fig. S6A), validating the adhesive and stimulatory properties of ASDCs in the CSF. Additionally, ASDCs were also overrepresented in the CSF of IDD patients compared with normal individuals ($p = 0.02$), implying the disease-associated characteristics of ASDCs (Fig. 5C). To locate and validate ASDC cells *in situ*, we also performed RNA single-molecule fluorescence *in situ* hybridization (smFISH) targeting *CD3*, *AXL*, and *SIGLEC6* in brain tissue sections of IDD patients (Fig. 5D, and fig. S6B to D). The presence of ASDCs in brain tissue of IDD patients were confirmed by the overlapping signal from the *AXL* and *SIGLEC6* RNA probes, and we also found several ASDCs colocalizing with the *CD3* RNA probe (Fig. 5D, and fig. S6C). Compared with normal brain tissue, ASDCs and *CD3*⁺ adjacent ASDCs also showed a notable increase in brain tissue of IDD patients (Fig. 5E, and fig. S6D). These findings support our *in silico* prediction of poly-adhesive, stimulatory, and disease-associated characteristics of ASDCs.

3.6. The early kinetics of ASDC induction are confirmed in the mouse model of autoimmune CNS inflammation

Considering the immunological network and the early increase of ASDCs in the CSF, we hypothesized that they might play a pro-inflammatory role in the early phase of the disease. To test this hypothesis, we investigated the kinetics of ASDCs in the mouse model

[52,53]. We utilized the previous FACS sorting scheme suggested for tDCs, the murine homologs of human ASDCs [27].

EAE was induced in mice with myelin oligodendrocyte glycoprotein (MOG) antigen. The disease onset and peak of disease severity after immunization are typically observed on days 11.4 ± 1.02 and 15.8 ± 1.94 , respectively. Therefore, in this study, mice were sacrificed 10 days and 15 days after immunization for tDC analysis in the EAE model to investigate the early phase of the disease (fig. S7, A and B).

Immune cells were isolated from the CNS (brain and spinal cord), spleen, and inguinal lymph node (inLN) tissues and stained for surface markers. CD3/CD19, Ly6G, F4/80, Xcr1, and CD11b were used as markers to eliminate other immune cells such as T cells, B cells, monocyte/macrophages, neutrophils, DC1s, and DC2s. tDCs and pDCs were separated by using the Cx3cr1 marker, and tDCs were divided into the Ly6c^{low} CD11c^{high} tDCs (referred to as CD11c^{high} tDCs) and the Ly6c^{high} CD11c^{low} tDCs (referred to as CD11c^{low} tDCs) populations as previously defined (fig. S7C) [27].

We compared the ratios of DC subsets in three groups (normal vs. EAE D-10 vs. EAE D-15) in the spleen, inLN, and CNS tissues. In the spleen, the frequency of CD11c^{high} tDCs and DC1s were increased in EAE D-10 compared with either normal control or EAE D-15 (fig. S7D). Moreover, the frequency of both types of tDCs and pDCs were increased in inLN of EAE D-10, when mice began to show symptoms of EAE. In contrast to the lymphoid organs, the frequency of all DC types in the CNS started to increase at day 10 and further increased as the EAE symptoms became severe (day 15, fig. S7, D and E). This finding is in accordance with the previous study of the mouse influenza infection model [27], where tDC numbers were increased shortly after the infection. Taken

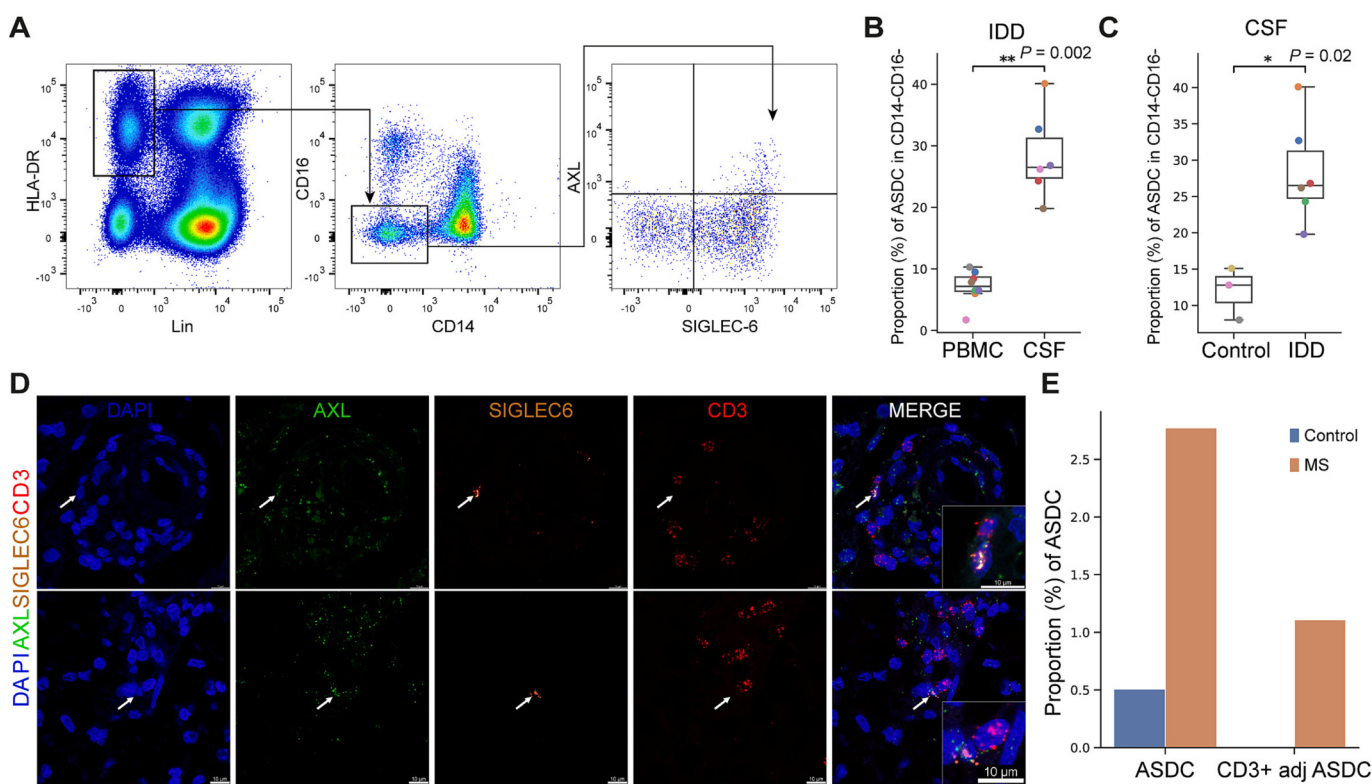


Fig. 5. ASDC identified by flow cytometry for CSF cells and RNA smFISH for brain biopsy tissues.

(A) Flow cytometry Gating strategy. Data is one of the representative experiments.

(B) Boxplot showing cell type proportion of ASDC between CSF and PBMC. p-values were calculated with the Mann–Whitney U test. * $p < 0.05$, ** $p < 0.01$, *** $p < 0.001$.

(C) Boxplot showing cell type proportion of ASDC between normal and MS patient. p-values were calculated with the Mann–Whitney U test. * $p < 0.05$, ** $p < 0.01$, *** $p < 0.001$.

(D) RNA smFISH detection of *AXL*, *SIGLEC6*, and *CD3* taken from two different sections of the brain tissue of an MS patient.

(E) Barplot showing the proportions of ASDCs in brain tissues between normal and MS patient.

together, our result supports the hypothesis that tDCs are involved in the early kinetics of the inflammatory response.

3.7. ASDCs are also increased in the pathological site of inflammatory bowel disease

As we found DCs overrepresented in the CSF in all three types of IDD, we reasoned that these cell types may also be present in other autoimmune diseases. Therefore, we searched the literature for accessible datasets for other diseases. Notably, we could identify all DCs overrepresented in the CSF in a previous scRNA-seq study of Crohn's disease with matched PBMCs and ileum (from both an involved and an uninvolved site) [54]. From this dataset, we performed subclustering of 9294 myeloid cells (PBMC $n = 5492$; non-involved ileum $n = 1428$; involved ileum $n = 2374$) and found 10 clusters (Fig. 6, A and B). Interestingly, all three DCs at higher levels in CSF (ASDC, ACY3⁺ DCs, and LAMP3⁺ DCs) were found in the dataset of Crohn's disease and marker genes in the DC subsets showed identical patterns as in our study (Fig. 6, C and D). When comparing the cell proportions between different conditions, we found that both ASDC and LAMP3⁺ DC numbers were higher at the involved site of the ileum compared with the non-involved site. In contrast, ACY3⁺ DCs were enriched in the non-involved site of the ileum compared with the involved site (Fig. 6, E and F). This confirms and generalizes the association of ASDCs with inflammatory diseases. Finally, we also analyzed the scRNA-seq study of PBMCs in MS patients treated with or without natalizumab, to seek for the presence of DCs overrepresented in CSF in PBMCs after natalizumab administration (fig. S8A) [12]. However, no clear cluster could be defined as DCs overrepresented in CSF, albeit some cells in the DC2 population were found to express *AXL* and *PPP1R14A* (fig. S8B). When we performed DEG analysis between natalizumab post-treatment and pre-treatment samples in the DC2 cluster, no significant change in ASDC marker gene expression levels could be found (fig. S8C). This result, and sparsity of ASDCs in PBMC samples, suggest that ASDCs in CSF might be differentiated within the CNS.

4. Discussion

In our scRNA-seq study of IDDs, we discovered the ASDC as a novel, disease-associated DC subtype, overrepresented in CSF, that forms an adhesive and stimulatory network with LAMP3⁺ DCs, together priming and activating various immune cells including CD4⁺ T cells and B cells, and orchestrating the inflammatory immune response. We highlight that these DCs overrepresented in CSF were also found in the ileum of inflammatory bowel disease patients. To the best of our knowledge, this study is the first to focus on ASDCs in the pathogenesis of IDDs and we emphasize the potential importance of ASDCs in the initiation and maintenance of these diseases.

ASDCs are a recently defined population that shares characteristics of both DC2 and pDC signatures [25]. We noticed an increase in ASDCs at the site of inflammation in both IDD and inflammatory bowel disease and validated their presence in the brain tissue of MS patient and mouse EAE model. Cell interaction analysis shows that ASDCs have the potential to activate LAMP3⁺ DCs and memory CD4⁺ T cells by expressing TNFSF9 and TNFSF15, respectively, and have a unique poly-adhesive function by expressing *CD5*, *CD72*, *NCAM1*, *ICAM4*, *ADAM33*, *VASN*, and *CDH1*. ASDCs were previously shown to stimulate T cell proliferation, superior to DC1s and DC2s [25]. *TNFSF15* may account for the superiority of ASDCs in stimulating T cells, since *TNFSF15* is strongly expressed only in ASDCs and ACY3⁺ DCs, in contrast to the costimulatory *CD86* molecule which is expressed in all subtypes of DCs. *TNFSF15* is additionally known to regulate vascular homeostasis and inflammation, Th1 cytokine production, and dendritic cell maturation, and together with its functional receptor TNFRSF25, they are involved in several chronic immunological disorders, including inflammatory bowel disease [55–57]. Considering the stimulatory role of TNFSF9 and

TNFSF15 in inflammation, neutralizing antibodies targeting these molecules may be compelling as a potential therapy for IDDs.

ASDCs express many adhesion molecules which are usually confined to specific cell types. For example, CD22 (Siglec-2) is usually expressed on B cells and binds to sialic acids in α 2,6 linkages, recognizing self-structures triggering inhibitory signals, and is also known to contribute to the regulation of autoimmunity [58]. In addition to the adhesive role of CDH1 (E-cadherin), E-cadherin is known to take part in the pathogenesis of T cell-mediated inflammation, and ICAM4 is also involved in immune cell recruitment to the site of inflammation by interacting with LFA-1 (ITGAL) and VLA-4 (ITGA4) [44,45]. On account of their poly-adhesive characteristics, ASDCs may play a pivotal role in the pathogenesis of IDDs by adhering to and triggering the inflammatory cascade of various immune cells.

ACY3⁺ DCs are a novel DC population that is overrepresented in CSF and has not previously been defined. ACY3⁺ DC numbers were increased in CSF without association with disease, in contrast to inflammatory bowel disease, in which ACY3⁺ DC numbers were increased in the uninflamed site of the ileum compared with the inflamed site. Further studies are required to define the functional role and association with autoimmune inflammatory disease of this novel DC population.

The LAMP3⁺ DC is an activated DC, characterized by *LAMP3* and *CCR7* expression [59,60]. The role and the importance of LAMP3⁺ DCs are being extensively studied in cancer [61–63], but only a few studies have examined their role in IDDs [20]. We have outlined the existence of LAMP3⁺ DCs in CSF at the single-cell level and described its role in activating B cells and T cells. Although LAMP3⁺ DCs were not increased in the CSF of IDD patients compared with that of non-inflammatory controls, the presence of ASDCs in the setting of inflammation may turn on LAMP3⁺ DCs to trigger various cell types. Elevated CCL19 levels have been found in the CSF of patients with recurrent and progressive MS, and increased levels of CXCL13 were associated with disease exacerbations and unfavorable prognosis in relapsing-remitting MS [64–66]. In our study, CCL19 and CXCL13 were strongly and exclusively expressed by LAMP3⁺ DCs, activating B cells in the CSF, which may lead to recurrent and progressive disease. Previous studies have demonstrated the migration of B cells from the periphery to CSF [67,68] and the differentiation of B cells in the CSF [69]. LAMP3⁺ DCs may account for this phenomenon, along with follicular helper T cells which were shown to enhance B cell enrichment [11], justifying the role of B cell-depleting therapies in MS [8,70].

Collectively, ASDCs and LAMP3⁺ DCs constitute an adherent and inflammatory core within the CNS, stimulating CD4⁺ T cells and B cells and thereby contributing to the pathogenesis of IDD. While we have identified ASDCs in proximity to T cells within the brain tissue of MS patient, further spatial mapping is necessary to investigate their specific locations and validate their co-localization with T and B cells. The comprehensive annotation of CNS immune cells in this study may serve as a valuable resource for future research endeavors.

Our study provides essential insight into a deeper understanding of the role of DCs in IDD pathology, highlighting the overrepresentation in the CSF and disease associations of the ASDC population. Considering its unique gene expression program and general association with inflammatory conditions, ASDC is a potential target for anti-inflammatory therapy.

Author contributions

D.Y-Y, M.H-K, and W.S-K performed experiments, J.H-K performed computational analysis. J.H-K, D.Y-Y, M.H-K, and W.S-K made contributions to the interpretation of data and prepared the first draft of the manuscript. S.M.K, J.E.P., and S.J.C conceived and supervised the study. All authors revised the draft critically for important intellectual content and gave final approval for the final manuscript version to be published.

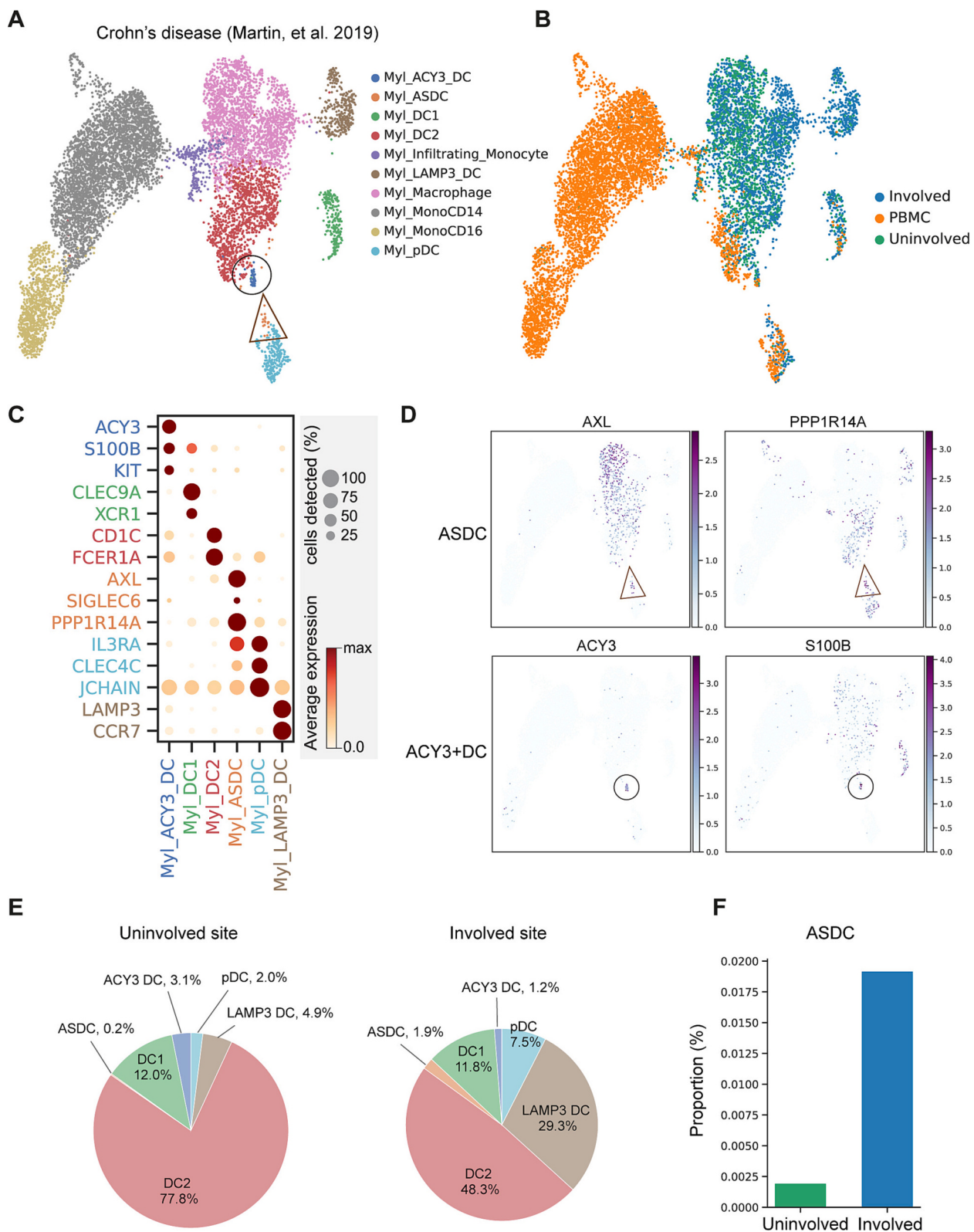


Fig. 6. Dendritic cell subtypes overrepresented in CSF are also identified in inflammatory bowel disease.

(A and B) UMAP plot of secondary clustering of myeloid cells ($n = 9294$) in the scRNA-seq study of Crohn's disease colored by cell types (A), and the site of sample collection (B).

(C) Dot plot for expression of marker genes in dendritic cell subtypes.

(D) UMAP plot showing marker gene expressions of ASDCs and ACY3⁺ DCs.

(E) Pie plot showing dendritic cell proportions between sample collection sites.

(F) Barplot showing the proportions of ASDCs between different sample collection sites.

Declaration of Competing Interest

S.M.K has lectured, consulted, and received honoraria from Bayer Schering Pharma, Genzyme, Merck Serono, and UCB; received a grant from the National Research Foundation of Korea and the Korea Health Industry Development Institute Research; is an Associate Editor of the Journal of Clinical Neurology. S.M.K and Seoul National University Hospital have transferred the technology of flow cytometric autoantibody assay to EONE Laboratory, Korea. The remaining authors declare no competing interests.

Data availability

The scRNA-seq data generated from this study have been deposited in the Gene Expression Omnibus repository with the accession code GSE194078. Technical scRNA-seq information and patient details are included as Supplementary Tables. Public scRNA-seq from MS and Crohn's disease were downloaded from GSE138266 (MS), GSE144744 (MS), and GSE134809 (Crohn's disease), respectively. The code for reproducing the single-cell sequencing results in this manuscript has been deposited at GitHub(<https://github.com/scmgl-kaist/IDScRNaseq2022>).

Acknowledgments

This work is supported by Grant No. HI21C0539 from the Korea Health Industry Development Institute Research Fund. Some of the biospecimens for this study were provided by the Seoul National University Hospital Human Biobank, a member of the Korea Biobank Network, which is supported by the Ministry of Health and Welfare. Junho Kang was supported by a grant of the MD-PhD/Medical Scientist Training Program through the Korea Health Industry Development Institute (KHIDI), funded by the Ministry of Health & Welfare, Republic of Korea. Jong-Eun Park was supported by the POSCO Science Fellowship.

Appendix A. Supplementary data

Supplementary data to this article can be found online at <https://doi.org/10.1016/j.clim.2023.109686>.

References

- [1] C.H. Polman, S.C. Reingold, B. Banwell, M. Clanet, J.A. Cohen, M. Filippi, K. Fujihara, E. Havrdova, M. Hutchinson, L. Kappos, F.D. Lublin, X. Montalban, P. O'Connor, M. Sandberg-Wollheim, A.J. Thompson, E. Waubant, B. Weinshenker, J.S. Wolinsky, Diagnostic criteria for multiple sclerosis: 2010 revisions to the McDonald criteria, *Ann. Neurol.* 69 (2011) 292–302.
- [2] D.K. Sato, D. Callegaro, M.A. Lana-Peixoto, P.J. Waters, F.M. de Haidar Jorge, T. Takahashi, I. Nakashima, S.L. Apostolos-Pereira, N. Talim, R.F. Simm, A.M. M. Lino, T. Misu, M.I. Leite, M. Aoki, K. Fujihara, Distinction between MOG antibody-positive and AQP4 antibody-positive NMO spectrum disorders, *Neurology*, 82 (2014) 474–481.
- [3] J. Kitley, P. Waters, M. Woodhall, M.I. Leite, A. Murchison, J. George, W. Küker, S. Chandrasekhar, A. Vincent, J. Palace, Neuromyelitis optica spectrum disorders with aquaporin-4 and myelin-oligodendrocyte glycoprotein antibodies: a comparative study, *JAMA Neurol.* 71 (2014) 276–283.
- [4] D.M. Wingerchuk, V.A. Lennon, S.J. Pittock, C.F. Lucchinetti, B.G. Weinshenker, Revised diagnostic criteria for neuromyelitis optica, *Neurology*, 66 (2006) 1485–1489.
- [5] J.Y. Hor, C.K. Wong, J.V. Ew, S. Idris, H.J. Tan, D.Y.J. Wong, Neuromyelitis optica spectrum disorder in Asia: epidemiology and risk factors, *Neurol. Clin. Neurosci.* 9 (2021) 274–281.
- [6] J.-E. Kim, S.-H. Park, K. Han, H.J. Kim, D.-W. Shin, S.-M. Kim, Prevalence and incidence of neuromyelitis optica spectrum disorder and multiple sclerosis in Korea, *Mult. Scler.* 26 (2020) 1837–1844.
- [7] S. Zamvil, P. Nelson, J. Trotter, D. Mitchell, R. Knobler, R. Fritz, L. Steinman, T-cell clones specific for myelin basic protein induce chronic relapsing paralysis and demyelination, *Nature*, 317 (1985) 355–358.
- [8] S.L. Hauser, A. Bar-Or, G. Comi, G. Giovannoni, H.-P. Hartung, B. Hemmer, F. Lublin, X. Montalban, K.W. Rammohan, K. Selcuk, A. Traboulsee, J.S. Wolinsky, D.L. Arnold, G. Klingelschmitt, D. Masterman, P. Fontoura, S. Belachew, P. Chin, N. Mairon, H. Garren, L. Kappos, OPERA I and OPERA II clinical investigators, Ocrelizumab versus interferon Beta-1a in relapsing multiple sclerosis, *N. Engl. J. Med.* 376 (2017) 221–234.
- [9] D.S. Reich, D.L. Arnold, P. Vermersch, A. Bar-Or, R.J. Fox, A. Matta, T. Turner, E. Wallström, X. Zhang, M. Mares, F.A. Khabirov, A. Traboulsee, Tolebrutinib phase 2b study group, safety and efficacy of tolebrutinib, an oral brain-penetrant BTK inhibitor, in relapsing multiple sclerosis: a phase 2b, randomised, double-blind, placebo-controlled trial, *Lancet Neurol.* 20 (2021) 729–738.
- [10] M.T. Cencioni, M. Mattoscio, R. Magliozzi, A. Bar-Or, P.A. Muraro, B cells in multiple sclerosis - from targeted depletion to immune reconstitution therapies, *Nat. Rev. Neurol.* 17 (2021) 399–414.
- [11] D. Schafflick, C.A. Xu, M. Hartlehert, M. Cole, A. Schulte-Mecklenbeck, T. Lautwein, J. Wolbert, M. Heming, S.G. Meuth, T. Kuhlmann, C.C. Gross, H. Wiendl, N. Yosef, G. Meyer Zu Horste, Integrated single cell analysis of blood and cerebrospinal fluid leukocytes in multiple sclerosis, *Nat. Commun.* 11 (2020) 247.
- [12] M. Kaufmann, H. Evans, A.-L. Schaupp, J.B. Engler, G. Kaur, A. Willing, N. Kursawe, C. Schubert, K.E. Attfield, L. Fugger, M.A. Friese, Identifying CNS-colonizing T cells as potential therapeutic targets to prevent progression of multiple sclerosis, *Med. (N.Y.)* 2 (2021) 296–312.e8.
- [13] D.A. Giles, P.C. Duncker, N.M. Wilkinson, J.M. Washnock-Schmid, B.M. Segal, CNS-resident classical DCs play a critical role in CNS autoimmune disease, *J. Clin. Invest.* 128 (2018) 5322–5334.
- [14] M.K. Mishra, V.W. Yong, Myeloid cells - targets of medication in multiple sclerosis, *Nat. Rev. Neurol.* 12 (2016) 539–551.
- [15] I. Ifergan, S.D. Miller, Potential for targeting myeloid cells in controlling CNS inflammation, *Front. Immunol.* 11 (2020), 571897.
- [16] E. Esau洛va, C. Cantoni, I. Shchukina, K. Zaitsev, R.C. Bucelli, G.F. Wu, M. N. Artyomov, A.H. Cross, B.T. Edelson, Single-cell RNA-seq analysis of human CSF microglia and myeloid cells in neuroinflammation, *Neurol. Neuroimmunol. Neuroinflamm.* 7 (2020), <https://doi.org/10.1212/NXI.0000000000000732>.
- [17] E. Kamma, W. Lasisi, C. Libner, H.S. Ng, J.R. Plemel, Central nervous system macrophages in progressive multiple sclerosis: relationship to neurodegeneration and therapeutics, *J. Neuroinflammation* 19 (2022) 45.
- [18] H. Drakesmith, B. Chain, P. Beverley, How can dendritic cells cause autoimmune disease? *Immunol. Today* 21 (2000) 214–217.
- [19] B. Ludewig, T. Junt, H. Hengartner, R.M. Zinkernagel, Dendritic cells in autoimmune diseases, *Curr. Opin. Immunol.* 13 (2001) 657–662, [https://doi.org/10.1016/s0952-7915\(01\)00275-8](https://doi.org/10.1016/s0952-7915(01)00275-8).
- [20] B. Serafini, B. Rosicarelli, R. Magliozzi, E. Stigliano, E. Capello, G.L. Mancardi, F. Aloisi, Dendritic cells in multiple sclerosis lesions: maturation stage, myelin uptake, and interaction with proliferating T cells, *J. Neuropathol. Exp. Neurol.* 65 (2006) 124–141.
- [21] F. Luessi, F. Zipp, E. Witsch, Dendritic cells as therapeutic targets in neuroinflammation, *Cell. Mol. Life Sci.* 73 (2016) 2425–2450.
- [22] M. Greter, F.L. Heppner, M.P. Lemos, B.M. Odermatt, N. Goebels, T. Laufer, R. J. Noelle, B. Becher, Dendritic cells permit immune invasion of the CNS in an animal model of multiple sclerosis, *Nat. Med.* 11 (2005) 328–334.
- [23] M. Alcántara-Hernández, R. Leyk, L.E. Wagar, E.G. Engleman, T. Keler, M. P. Marinkovich, M.M. Davis, G.P. Nolan, J. Idoiyaga, High-dimensional phenotypic mapping of human dendritic cells reveals interindividual variation and tissue specialization, *Immunity*, 47 (2017) 1037–1050.e6.
- [24] P. See, C.-A. Dutertre, J. Chen, P. Günther, N. McGovern, S.E. Irac, M. Gunawan, M. Beyer, K. Händler, K. Duan, H.R.B. Sumath, N. Ruffin, M. Jouve, E. Gea-Mallorquí, R.C.M. Hennekam, T. Lim, C.C. Yip, M. Wen, B. Malleret, I. Low, N. B. Shadan, C.F.S. Fen, A. Tay, J. Lum, F. Zolezzi, A. Larbi, M. Poidinger, J.K. Y. Chan, Q. Chen, L. Réna, M. Haniffa, P. Benaroch, A. Schlitzer, J.L. Schultz, E. W. Newell, F. Ginhoux, Mapping the human DC lineage through the integration of high-dimensional techniques, *Science*, 356 (2017), <https://doi.org/10.1126/science.aag3009>.
- [25] A.-C. Villani, R. Satija, G. Reynolds, S. Sarkizova, K. Shekhar, J. Fletcher, M. Griesbeck, A. Butler, S. Zheng, S. Lazo, L. Jardine, D. Dixon, E. Stephenson, E. Nilsson, I. Grundberg, D. McDonald, A. Fiby, W. Li, P.L. De Jager, O. Rozenblatt-Rosen, A.A. Lane, M. Haniffa, A. Regev, N. Hacohen, Single-cell RNA-seq reveals new types of human blood dendritic cells, monocytes, and progenitors, *Science*, 356 (2017), <https://doi.org/10.1126/science.aah4573>.
- [26] H. Zhang, J.D. Gregorio, T. Iwahori, X. Zhang, O. Choi, L.L. Tolentino, T. Prestwood, Y. Carmi, E.G. Engleman, A distinct subset of plasmacytoid dendritic cells induces activation and differentiation of B and T lymphocytes, *Proc. Natl. Acad. Sci. U. S. A.* 114 (2017) 1988–1993.
- [27] R. Leyk, M. Alcántara-Hernández, Z. Lanzar, A. Lüdtke, O.A. Perez, B. Reizis, J. Idoiyaga, Integrated cross-species analysis identifies a conserved transitional dendritic cell population, *Cell Rep.* 29 (2019) 3736–3750.e8.
- [28] Y.-L. Chen, T. Gomes, C.S. Hardman, F.A. Vieira Braga, D. Gutowska-Owiak, M. Salimi, N. Gray, D.A. Duncan, G. Reynolds, D. Johnson, M. Salio, V. Cerundolo, J.L. Barlow, A.N.J. McKenzie, S.A. Teichmann, M. Haniffa, G. Ogg, Re-evaluation of human BDCA-2+ DC during acute sterile skin inflammation, *J. Exp. Med.* 217 (2020), <https://doi.org/10.1084/jem.20190811>.
- [29] D.M. Wingerchuk, B. Banwell, J.L. Bennett, P. Cabre, W. Carroll, T. Chitnis, J. de Seze, K. Fujihara, B. Greenberg, A. Jacob, S. Jarius, M. Lana-Peixoto, M. Levy, J. H. Simon, S. Tenembaum, A.L. Traboulsee, P. Waters, K.E. Wellik, B. G. Weinshenker, International panel for NMO diagnosis, international consensus diagnostic criteria for neuromyelitis optica spectrum disorders, *Neurology*, 85 (2015) 177–189.
- [30] A.S. López-Chiriboga, M. Majed, J. Fryer, D. Dubey, A. McKeon, E.P. Flanagan, J. Jitrapapakulsan, N. Kothapalli, J.-M. Tillema, J. Chen, B. Weinshenker, D. Wingerchuk, J. Sagen, A. Gadoth, V.A. Lennon, B.M. Keegan, C. Lucchinetti, S.

- J. Pittock, Association of MOG-IgG Serostatus with relapse after acute disseminated encephalomyelitis and proposed diagnostic criteria for MOG-IgG-associated disorders, *JAMA Neurol.* 75 (2018) 1355–1363.
- [31] E.H. Sohn, S.-H. Jeong, Diagnosis of multiple sclerosis: 2017 McDonald diagnostic criteria, *J. Korean Neurol. Assoc.* 36 (2018) 273–279.
- [32] F.A. Wolf, P. Angerer, F.J. Theis, SCANPY: large-scale single-cell gene expression data analysis, *Genome Biol.* 19 (2018) 15.
- [33] S.L. Wolock, R. Lopez, A.M. Klein, Scrublet: computational identification of cell doublets in single-cell transcriptomic data, *Cell Syst.* 8 (2019) 281–291.e9.
- [34] I. Korsunsky, N. Millard, J. Fan, K. Slowikowski, F. Zhang, K. Wei, Y. Baglaenko, M. Brenner, P.-R. Loh, S. Raychaudhuri, Fast, sensitive and accurate integration of single-cell data with harmony, *Nat. Methods* 16 (2019) 1289–1296.
- [35] M. Efremova, M. Vento-Tormo, S.A. Teichmann, R. Vento-Tormo, CellPhoneDB: inferring cell-cell communication from combined expression of multi-subunit ligand-receptor complexes, *Nat. Protoc.* 15 (2020) 1484–1506.
- [36] R. Browaeys, W. Saelens, Y. Saeyns, NicheNet: modeling intercellular communication by linking ligands to target genes, *Nat. Methods* 17 (2020) 159–162.
- [37] P. Bankhead, M.B. Loughrey, J.A. Fernández, Y. Dombrowski, D.G. McArt, P. D. Dunne, S. McQuaid, R.T. Gray, L.J. Murray, H.G. Coleman, J.A. James, M. Salto-Tellez, P.W. Hamilton, QuPath: open source software for digital pathology image analysis, *Sci. Rep.* 7 (2017) 16878.
- [38] J. Villar, E. Segura, Decoding the heterogeneity of human dendritic cell subsets, *Trends Immunol.* 41 (2020) 1062–1071.
- [39] S.S. Iyer, G. Cheng, Role of interleukin 10 transcriptional regulation in inflammation and autoimmune disease, *Crit. Rev. Immunol.* 32 (2012) 23–63.
- [40] J.H. Kim, Y. Hu, T. Yongqing, J. Kim, V.A. Hughes, J. Le Nours, E.A. Marquez, A. W. Purcell, Q. Wan, M. Sugita, J. Rossjohn, F. Winau, CD1a on Langerhans cells controls inflammatory skin disease, *Nat. Immunol.* 17 (2016) 1159–1166.
- [41] F.A. Wolf, F.K. Hamey, M. Plass, J. Solana, J.S. Dahlin, B. Göttgens, N. Rajewsky, L. Simon, F.J. Theis, PAGA: graph abstraction reconciles clustering with trajectory inference through a topology preserving map of single cells, *Genome Biol.* 20 (2019) 59.
- [42] H. Van de Velde, I. von Hoegen, W. Luo, J.R. Parnes, K. Thielemans, The B-cell surface protein CD72/Lyb-2 is the ligand for CD5, *Nature*. 351 (1991) 662–665.
- [43] J. Van den Bossche, B. Malissen, A. Mantovani, P. De Baetselier, J.A. Van Ginderachter, Regulation and function of the E-cadherin/catenin complex in cells of the monocyte-macrophage lineage and DCs, *Blood*. 119 (2012) 1623–1633.
- [44] K.R.R. Siddiqui, S. Laffont, F. Powrie, E-cadherin marks a subset of inflammatory dendritic cells that promote T cell-mediated colitis, *Immunity*. 32 (2010) 557–567.
- [45] H. Yusuf-Makagiansar, M.E. Anderson, T.V. Yakovleva, J.S. Murray, T.J. Sahaan, Inhibition of LFA-1/ICAM-1 and VLA-4/VCAM-1 as a therapeutic approach to inflammation and autoimmune diseases, *Med. Res. Rev.* 22 (2002) 146–167.
- [46] J. Greenwood, Y. Wang, V.L. Calder, Lymphocyte adhesion and transendothelial migration in the central nervous system: the role of LFA-1, ICAM-1, VLA-4 and VCAM-1, *Off. Immunology*. 86 (1995) 408–415.
- [47] T. Futagawa, H. Akiba, T. Kodama, K. Takeda, Y. Hosoda, H. Yagita, K. Okumura, Expression and function of 4-1BB and 4-1BB ligand on murine dendritic cells, *Int. Immunopharmacol.* 14 (2002) 275–286.
- [48] D. Laderach, A. Wesa, A. Galy, 4-1BB-ligand is regulated on human dendritic cells and induces the production of IL-12, *Cell. Immunol.* 226 (2003) 37–44.
- [49] T.H. Schreiber, E.R. Podack, Immunobiology of TNFSF15 and TNFRSF25, *Immunol. Res.* 57 (2013) 3–11.
- [50] J. Borst, J. Hendriks, Y. Xiao, CD27 and CD70 in T cell and B cell activation, *Curr. Opin. Immunol.* 17 (2005) 275–281.
- [51] J. Denoed, M. Moser, Role of CD27/CD70 pathway of activation in immunity and tolerance, *J. Leukoc. Biol.* 89 (2011) 195–203.
- [52] C.S. Constantinescu, N. Farooqi, K. O'Brien, B. Gran, Experimental autoimmune encephalomyelitis (EAE) as a model for multiple sclerosis (MS), *Br. J. Pharmacol.* 164 (2011) 1079–1106.
- [53] B.A. 'tHart, B. Gran, R. Weissert, EAE: imperfect but useful models of multiple sclerosis, *Trends Mol. Med.* 17 (2011) 119–125.
- [54] J.C. Martin, C. Chang, G. Boschetti, R. Ungaro, M. Giri, J.A. Grout, K. Gettler, L.-S. Chuang, S. Nayar, A.J. Greenstein, M. Dubinsky, L. Walker, A. Leader, J.S. Fine, C.E. Whitehurst, M.L. Mbow, S. Kugathasan, L.A. Denson, J.S. Hyams, J. Friedman, P.T. Desai, H.M. Ko, I. Laface, G. Akturk, E.E. Schadt, H. Salmon, S. Gnjatic, A.H. Rahman, M. Merad, J.H. Cho, E. Kenigsberg, Single-cell analysis of Crohn's disease lesions identifies a pathogenic cellular module associated with resistance to anti-TNF therapy, *Cell*. 178 (2019) 1493–1508.e20.
- [55] Z. Zhang, L.-Y. Li, TNFSF15 modulates neovascularization and inflammation, *Cancer Microenviron.* 5 (2012) 237–247.
- [56] S. Jin, J. Chin, S. Seeber, J. Niewoehner, B. Weiser, N. Beaucamp, J. Woods, C. Murphy, A. Fanning, F. Shanahan, K. Nally, R. Kajekar, A. Salas, N. Planell, J. Lozano, J. Panes, H. Parmar, J. DeMartino, S. Narula, D.A. Thomas-Karyat, TL1A/TNFSF15 directly induces proinflammatory cytokines, including TNF α , from CD3 CD161 T cells to exacerbate gut inflammation, *Mucosal Immunol.* 6 (2013) 886–899, <https://doi.org/10.1038/mi.2012.124>.
- [57] V. Valatas, G. Kolios, G. Bamias, TL1A (TNFSF15) and DR3 (TNFRSF25): a co-stimulatory system of cytokines with diverse functions in gut mucosal immunity, *Front. Immunol.* 10 (2019) 583.
- [58] E.A. Clark, N.V. Giltay, CD22: a regulator of innate and adaptive B cell responses and autoimmunity, *Front. Immunol.* 9 (2018) 2235.
- [59] J.-E. Park, R.A. Bottig, C. Dominguez Conde, D.-M. Popescu, M. Lavaert, D. J. Kunz, I. Goh, E. Stephenson, R. Ragazzini, E. Tuck, A. Wilbrey-Clark, K. Roberts, V.R. Kedlian, J.R. Ferdinand, X. He, S. Webb, D. Maunder, N. Vandamme, K. T. Mahbubani, K. Polanski, L. Mamanova, L. Bolt, D. Crossland, F. de Rita, A. Fuller, A. Filby, G. Reynolds, D. Dixon, K. Saeb-Parsy, S. Ligso, D. Henderson, R. Vento-Tormo, O.A. Bayraktar, R.A. Barker, K.B. Meyer, Y. Saeyns, P. Bonfanti, S. Behjati, M.R. Clatworthy, T. Taghon, M. Haniffa, S.A. Teichmann, A cell atlas of human thymic development defines T cell repertoire formation, *Science*. 367 (2020), <https://doi.org/10.1126/science.aaay3224>.
- [60] N. Watanabe, Y.-H. Wang, H.K. Lee, T. Ito, Y.-H. Wang, W. Cao, Y.-J. Liu, Hassall's corpuscles instruct dendritic cells to induce CD4+CD25+ regulatory T cells in human thymus, *Nature*. 436 (2005) 1181–1185.
- [61] R. Sun, X. Wang, H. Zhu, H. Mei, W. Wang, S. Zhang, J. Huang, Prognostic value of LAMP3 and TP53 overexpression in benign and malignant gastrointestinal tissues, *Oncotarget*. 5 (2014) 12398–12409.
- [62] A. Nagelkerke, H. Mujcic, J. Bussink, B.G. Wouters, H.W.M. van Laarhoven, F.C.G. J. Sweep, P.N. Span, Hypoxic regulation and prognostic value of LAMP3 expression in breast cancer, *Cancer*. 117 (2011) 3670–3681.
- [63] X. Liao, Y. Chen, D. Liu, F. Li, X. Li, W. Jia, High expression of LAMP3 is a novel biomarker of poor prognosis in patients with esophageal squamous cell carcinoma, *Int. J. Mol. Sci.* 16 (2015) 17655–17667.
- [64] R. Gold, A. Jawad, D.H. Miller, D.C. Henderson, A. Fassas, W. Fierz, H.P. Hartung, Expert opinion: guidelines for the use of natalizumab in multiple sclerosis patients previously treated with immunomodulating therapies, *J. Neuroimmunol.* 187 (2007) 156–158.
- [65] M. Pashenkov, M. Söderström, H. Link, Secondary lymphoid organ chemokines are elevated in the cerebrospinal fluid during central nervous system inflammation, *J. Neuroimmunol.* 135 (2003) 154–160.
- [66] M. Khademi, I. Kockum, M.L. Andersson, E. Iacobaeus, L. Brundin, F. Sellebjerg, J. Hillert, P. Piehl, T. Olsson, Cerebrospinal fluid CXCL13 in multiple sclerosis: a suggestive prognostic marker for the disease course, *Mult. Scler.* 17 (2011) 335–343.
- [67] H.-C. von Büdingen, T.C. Kuo, M. Sirota, C.J. van Belle, L. Apeltsin, J. Glanville, B. A. Cree, P.-A. Gourraud, A. Schwartzburg, G. Huerta, D. Telman, P.D. Sundar, T. Casey, D.R. Cox, S.L. Hauser, B cell exchange across the blood-brain barrier in multiple sclerosis, *J. Clin. Invest.* 122 (2012) 4533–4543.
- [68] E.L. Eggers, B.A. Michel, H. Wu, S.-Z. Wang, C.J. Bevan, A. Abounasr, N.S. Pierson, A. Bischof, M. Kazer, E. Leitner, A.L. Greenfield, S. Demuth, M.R. Wilson, R. G. Henry, B.A. Cree, S.L. Hauser, H.-C. von Büdingen, Clonal relationships of CSF B cells in treatment-naïve multiple sclerosis patients, *JCI Insight*. 2 (2017), <https://doi.org/10.1172/jci.insight.92724>.
- [69] A. Corcione, S. Casazza, E. Ferretti, D. Giunti, E. Zappia, A. Pistorio, C. Gambini, G. L. Mancardi, A. Uccelli, V. Pistoia, Recapitulation of B cell differentiation in the central nervous system of patients with multiple sclerosis, *Proc. Natl. Acad. Sci. U. S. A.* 101 (2004) 11064–11069.
- [70] S.L. Hauser, E. Waubant, D.L. Arnold, T. Vollmer, J. Antel, R.J. Fox, A. Bar-Or, M. Panzara, N. Sarkar, S. Agarwal, A. Langer-Gould, C.H. Smith, HERMES trial group, B-cell depletion with rituximab in relapsing-remitting multiple sclerosis, *N. Engl. J. Med.* 358 (2008) 676–688.